

The high-resolution vertical structure of internal tides and near-inertial waves measured with an ADCP over the continental slope in the Bay of Biscay

Hendrik M. van Aken*, Hans van Haren, Leo R.M. Maas

Royal Netherlands Institute for Sea Research, P.O.Box 59, 1790 AB Den Burg, the Netherlands

Received 15 November 2004; received in revised form 23 March 2006; accepted 21 July 2006

Available online 1 February 2007

Abstract

ADCP measurements of the velocity structure in the permanent thermocline at two locations over the continental slope in the Bay of Biscay are presented. The vertical variation of the contribution of the inertia-gravity waveband to the kinetic energy, vertical motion, and current shear are analysed. The semi-diurnal tides together with near-inertial waves appear to provide over 70% of the high-frequency kinetic energy ($> 1/3$ cpd). Over the vertical range of the ADCP observations the phase of the harmonic M_2 tide changes up to 155° , while the kinetic energy varies in the vertical by a factor of 3.8, showing the importance of the contribution of internal waves to the observed tidal motion. Both semi-diurnal internal tidal waves and near-inertial waves have a vertically restricted distribution of the variance of the horizontal and vertical velocity, as in internal wave beams. The short-term 14-day averaged amplitude and phase lag of the M_2 tide shows large temporal changes, with a characteristic 40–45 day time scale. These changes are probably related to variations in generation sites and propagation paths of the internal tide, because of changes in the temperature and salinity stratification due to the presence of meso-scale eddies. The relatively large shear in the inertia-gravity wave band, mainly at near-inertial frequencies, supports low-gradient Richardson numbers that are well below 1 for nearly half of the time. This implies that the large shear may support turbulent mixing for a large part of the time.

© 2007 Elsevier Ltd. All rights reserved.

Keywords: Internal waves; Internal tides; Near-inertial waves; Bay of Biscay; Continental slope

1. Introduction

Internal inertia-gravity waves are waves where pressure changes due to density variations in the earth's gravity field as well as the Coriolis force contribute to the acceleration of water particles.

According to traditional theory, these waves can exist in the angular frequency (ω) band $f(\phi) < \omega < N(z)$ (Krauss, 1966). Here $f(\phi)$ is the local inertial or Coriolis frequency, $f(\phi) = 2\Omega \sin(\phi)$, twice the local vertical component of the earth rotation vector Ω at latitude ϕ , and $N(z)$ is the depth-dependent Brunt-Väisälä or buoyancy frequency, which depends on the adiabatic density gradient: $N^2(z) = (-g \, d \ln(\rho) / dz)_{\text{ad}}$ with g the gravitational acceleration and ρ the time averaged water

*Corresponding author. Tel.: +31 222 369 416;
fax: +31 222 319 674.

E-mail address: aken@nioz.nl (H.M. van Aken).

density. Such waves contribute significantly to the kinetic energy in the abyssal Bay of Biscay (Pingree and New, 1991, 1995; van Haren et al., 2002). These waves, especially at tidal and near-inertial frequencies, are assumed to be a main agent for the transport of mechanical energy into the deep abyssal ocean worldwide. There the wave energy can be converted to turbulent kinetic energy available for diapycnal mixing that drives the global deep upwelling (Munk and Wunsch, 1998). Over the slopes of the Mid-Atlantic Ridge in the Brazil Basin, high levels of turbulence were observed, attributed to the breaking of internal waves that were generated by tidal currents flowing over the irregular steep topography of this ridge (Polzin et al., 1997; Ledwell et al., 2000).

Internal waves can be described in different ways. For a horizontally homogeneous ocean with a flat bottom, Vertical modes (vertically standing waves) are used to describe the internal waves with the largest vertical scales (Fjeldstad, 1963). If the vertical wavelength of these waves reduces to scales smaller than the scale of vertical variation of the density stratification, nearly plane internal waves can be assumed to be slowly modulated so that the vertically changing stratification influences only the local vertical wavelength, phase and group velocity, and does not lead to energy scattering and trapping: the WKB approximation (Leblond and Mysak, 1978). When internal waves of certain frequency are locally generated over steep topography, e.g. as internal tides, the waves can no longer be approximated as nearly plane waves or vertical modes. Then the propagation of wave energy can be analysed by the method of ray tracing. There the mechanical energy of the internal waves is assumed to be spatially concentrated in narrow beams that may reflect at the sea surface or at the bottom of the ocean (e.g. Thomas and Stevenson, 1972; Baines, 1982; Gerkema, 2001). In a wave beam the concept of wavelength, developed for plane waves, fails, since the beam is a superposition of a large number of plane wave modes (Lighthill, 1978). However, one can still define a characteristic length scale, the distance over which extrapolation of the observed phase shift would reach a value of 360° . In the case of plane waves this length scale equals the wavelength.

Garrett and Munk (1972, 1975) devised a semi-empirical universal spectral model (GM spectrum) for the statistical description of the internal wave field in the abyssal ocean. For this model the

existence of a vertical modal structure of the internal waves was not vital. A basic assumption for the model was horizontal statistical isotropy, for which strong non-linear resonant interaction to redistribute energy among wave numbers and frequencies would be expected. The model assumes no vertical or horizontal flux of mechanical energy and a perfectly reflecting smooth horizontal ocean bottom. The resulting model spectrum was presented as an equivalent continuum spectrum, without any spectral lines at tidal frequencies.

Shortly after the Garrett–Munk spectrum was introduced, Hayes and Halpern (1976) presented evidence that near the continental slope off Oregon the bulk of the kinetic energy of internal waves was not smoothly distributed over the frequencies, as in the GM spectrum, but was found in the spectral bands near the semi-diurnal and inertial frequencies. The kinetic energy level in these bands was not stationary but appeared to vary over time by an order of magnitude. From temperature observations in the deep Bay of Biscay, Pingree and New (1991) found evidence that the energy of semi-diurnal internal tides propagated from their generation area near the continental break into the open ocean. There the internal wave beam reflected at the bottom. Gerkema (2001) has theoretically shown that variation in the seasonal stratification may lead to changes in the propagation and structure of internal wave beams in the Bay of Biscay. It can be expected that stratification changes due to the presence of meso-scale eddies will lead to similar variations in the internal wave structure.

In this paper, we focus on the vertical and temporal structure of semi-diurnal internal tides and near-inertial waves in the main thermocline over the continental slope in the Bay of Biscay. Observations and modelling efforts have shown that internal tidal waves are generated at the continental break and propagate mainly downward as an 800 m thick wave beam (Pingree and New, 1991; Lam et al., 2004; Gerkema et al., 2004). The available data set consists of two moored ADCP records from 1995–96 and 1997–98 of the horizontal and vertical velocity components (Table 1). The length of each record is about 1 year, which allows accurate estimates of the internal wave statistics in the inertial and semi-diurnal frequency bands. Additionally, data from a current meter mounted near the bottom at BB 17 (Fig. 1) were used. The high vertical resolution of the ADCP observations, compared with classic current meters, allows the

Table 1
Information on the TripleB ADCP Moorings

Moorings	Longitude	Latitude	Water depth (m)	Bin range (m)	Bin size (m)	Sampling period (min)	Ensemble (pings)	Start date	Number of days
BB 1	5°22'W	46°43'N	1615	1075–723	16	15	80	20 July 1995	336
BB 17	8°17'W	47°38'N	1498	970–602	8	30	190	15 August 1997	370

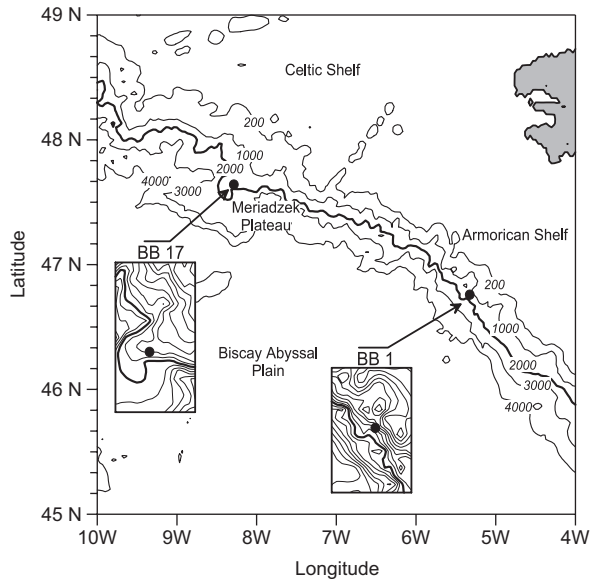


Fig. 1. Bathymetry (m) of the northern Bay of Biscay with the positions of the ADCP moorings. The insets show details of the topography with depth contours every 200 m. The 2000 m isobath is highlighted as a thick line.

analysis of the vertical change of amplitude and phase of internal waves and the inference of wave beams. Attention is given to the permanent vertical structure of the M_2 internal tides as well as to the variable part of the internal tides. The spectral behaviour of the current shear, inherent in the internal and inertial waves, is analysed too, since such wave shear may drive the turbulence and turbulent mixing in the thermocline.

2. The data

As part of the Dutch “TripleB” research programme between 1995 and 1998, a moored ADCP was deployed at two locations in the Bay of Biscay for about 1 year in each deployment. The two sites, both near the 1500 m isobath on the continental slope (Fig. 1), were separated by 240 km. The

upward looking four-beam 76.8 kHz narrow-band ADCP, manufactured by RDI, was mounted on the mooring so that the observational range of the instrument (about 400 m) covered the permanent thermocline. In the observational depth range the acoustic backscatter generally was relatively high over the year, because of the presence of a deep scattering layer with the highest amounts of scatterers in the shallower levels of the observational range. The instrument was fitted with an additional external battery pack, in order to increase the number of pings in the recorded ensembles. Horizontal and vertical velocity components and an error velocity were obtained from the ADCP. The latter was used as a measure for the accuracy of the velocity measurements. For mooring BB 1 ensemble averages of 80 pings were recorded every 15 min, from which the velocity components were derived in 25 bins, each 16 m in range. The data from ADCP bin 1 of mooring BB 1 showed many spikes because of the occasional presence of a pick-up buoy in one of the ADCP beams, while bin 25 at the end of the observational range showed many outliers. These bins were not used for further analysis because of their limited quality. The 15 min ensemble average of the error velocity of bins 2–24 had a standard deviation of 0.9 cm s^{-1} . This agrees with the white noise level, derived from the spectra of the vertical velocity, presented below. The error level hardly increased from bins 2 to 24. For mooring BB 17 the number of pings in each ensemble was increased to 190, recorded every 30 min in 50 bins of 8-m length. For this mooring bins 1 and 2 were of limited quality because of interference with the pick-up buoy, while the last bin, bin 50, had many outliers. These three bins were also discarded for further analysis. The standard deviation of the ensemble average of the error velocity in the remaining bins was only 0.3 cm s^{-1} and hardly varied with depth. While the position of mooring BB 1 was reasonably unobstructed by topography on the continental

slope, mooring BB 17 was situated along a curving promontory of the Meriadzek Plateau. In both cases irregular topography, with canyons cutting into the continental slope, was nearby. A summary of the main ADCP settings is given in Table 1.

Nearby CTD stations, occupied before the deployment and after the recovery of the ADCP moorings, were used to determine the mean stability structure for both moorings. The 400-m ADCP beams were located in the main thermocline, which was found at pressure levels between 500 and 1100 dbar. Maximum mean values of the Brunt-Väisälä frequency, N , in the main thermocline (38 and 43 cpd) were observed near 800 dbar (Fig. 2). Above the main thermocline a thermostad was present with a Brunt-Väisälä frequency of about 25 cpd in the 200- to 400-dbar interval. The shallow N maximum near a pressure of 50 dbar was not reached by our observations. Note for comparison that the local Coriolis frequency equals about 1.5 cpd. In these circumstances semi-diurnal tides,

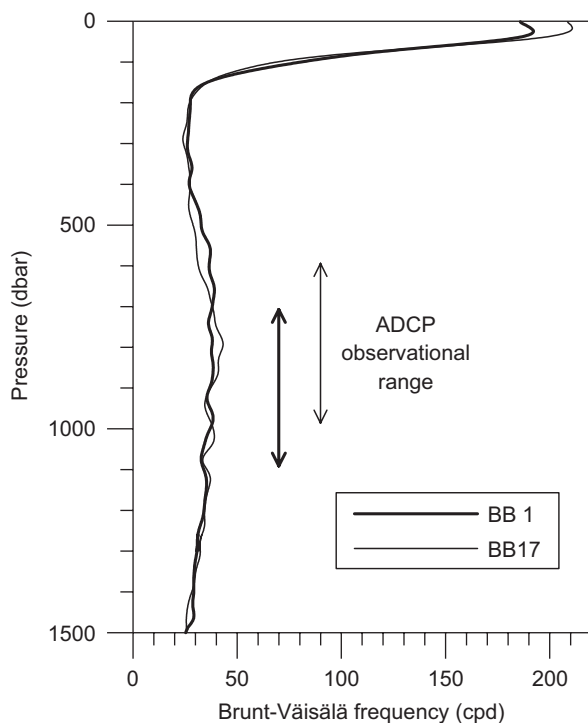


Fig. 2. Profiles of the Brunt-Väisälä frequency for moorings BB 1 (thick line) and BB 17 (thin line). These profiles are based on the average of 8 (BB 1) or 7 (BB 17) nearby CTD stations occupied before deployment or after recovery of the moorings. In the calculation of this frequency, the adiabatic density gradient was estimated from 50 dbar vertical differences. The observational ranges of the ADCP are indicated with the two-headed arrows.

with frequency $\omega \approx 2$ cpd and $f < \omega < N$, can exist as free internal waves.

Interference of a vertically propagating internal tidal wave and a barotropic tide may generate a vertical structure of the net tidal amplitude and phase lag that hides the true structure of the internal tide. For the interpretation of our observations as representative for baroclinic tides, an estimate of the magnitude of the barotropic tide is required. With only data from a 400 m observational range and a local ocean depth of about 1500 m, a strict separation between barotropic and baroclinic waves is not possible. Measurements of barotropic tides over the continental slope in the Bay of Biscay are scarce. Along the continental slope the strength of the barotropic tide varies considerably in strength (Pingree et al., 1983). Pérenne and Pichon (1999) have determined the barotropic tidal amplitudes with a bottom-mounted ADCP near the 300 m isobath at two positions, within 65 and 40 km of our moorings BB 1 and 17, respectively. When we assume that the barotropic mass flux connected with these tidal currents is constant over the continental slope, the major and minor semi-axes of the M_2 tidal ellipse are ~ 6 and 5 cm s^{-1} and 4 and 2 cm s^{-1} for the vicinity of moorings BB 1 and 17, respectively. Measurements with a towed ADCP for ~ 24 h along three cross-slope sections, located between the moorings of Pérenne and Pichon (1999), reported by Lam et al. (2004) confirmed the existence of internal wave beams at semi-diurnal frequencies. Below 500 m depth the baroclinic velocity amplitudes were stronger than those of the barotropic tide. Those measurements also have confirmed that indeed the tidal mass transport is constant over the continental slope within 30%. The observed along-slope gradient in the barotropic semi-diurnal tidal amplitudes by Lam et al. (2004) confirms the modelling results of Pingree et al. (1983). This implies that at the BB 1 position the M_2 barotropic tide is probably weaker than derived from the results of Pérenne and Pichon (1999). The mean cross-slope and along-slope tidal amplitudes at BB 1, estimated from extrapolation of the results of Lam et al. (2004), suggest a barotropic semi-diurnal tidal flow with cross-slope and along-slope amplitudes of 6 and 1 cm s^{-1} , respectively. Probably the M_2 tidal components at BB 1 are even smaller since the observations by Lam et al. (2004) have a spring tide bias. The available phase information of the barotropic M_2 tide near our moorings is not accurate enough to allow subtraction of the

barotropic tide from the ADCP observations. Therefore, the original data were analysed, being a mixture of barotropic and baroclinic motions. However, most likely the magnitudes of the variance of orthogonal current components of the barotropic M_2 tide estimated from the observations presented here amount to about $20\text{ cm}^2\text{ s}^{-2}$ and $10\text{ cm}^2\text{ s}^{-2}$ or less for moorings BB 1 and 17, respectively.

3. Results

3.1. Horizontal velocity spectra

In order to illustrate the characteristic contribution of tidal and other frequencies to the observed horizontal motion in the permanent thermocline, we have determined vertically averaged power spectra for the horizontal and vertical motion observed with the ADCPs. Spectra were determined for successive 70-day periods with a 35-day overlap

and averaged subsequently. End-point matching for each 70-day period was used as a data windowing technique in order to prevent smearing of tidal and inertial spectral peaks due to side lobe leakage (Frankignoul, 1974). The resulting spectra, with about 10 degrees of freedom, were then averaged over all available ADCP bins. The total number of degrees of freedom in these averaged spectra, approximated following Shcherbina et al. (2003, Appendix) and Bendat and Piersol (1986), amounted to at least 120, reflecting an accurate spectral estimate.

The spectra for the east and north components were summed to obtain information on the frequency distribution of the kinetic energy. The resulting power spectra (Fig. 3) show a spectral continuum with, contrary to the smooth Garrett–Munk spectrum, a series of spectral lines in the frequency range up to 20 cpd for mooring BB 1 and up to 12 cpd for mooring BB 17. The dominant spectral lines were located at the M_2 and S_2

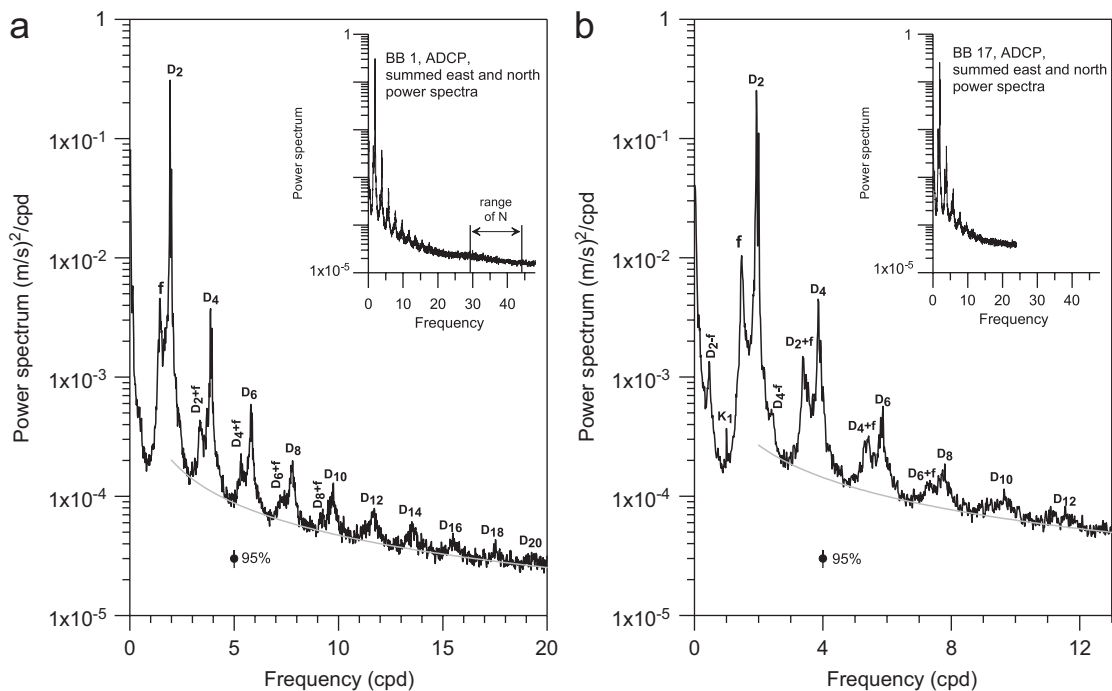


Fig. 3. Mean power spectra of the horizontal velocity, obtained by summing the power spectra of the east and north velocity components. The spectral estimates per bin, with 10 degrees of freedom, were averaged over bins 2 to 24 of mooring BB 1 (a) and bins 3 to 49 of mooring BB 17 (b). The indicated 95% confidence interval is a worst case estimate according to Shcherbina et al. (2003). The insets show the complete spectra, the main figure the part of the spectra with pronounced peaks. In the inset of mooring BB 1 the range of the Brunt-Väisälä frequency N (mean plus or minus twice the standard deviation) in the observational range is indicated with a two-headed arrow. That frequency range was not resolved for mooring BB 17 because of the 30 min sampling. The spectral peaks are indicated as semi-diurnal (D_2), inertial (f) or a higher harmonic for these frequency bands. The grey line illustrates the $\omega^{-0.9}$ character of the background spectral continuum.

semi-diurnal (D_2) tidal frequencies. The third highest spectral peak in the internal wave band spectra of the horizontal velocity was observed near the Coriolis frequency, f , indicative for near-inertial waves. At near multiples of the semi-diurnal frequency a regular pattern of peaks was observed, primarily consisting of a linear combination of higher harmonics of the semi-diurnal tidal frequencies (D_{2n} , $n = 1, 2, \dots$). Additional spectral peaks were observed at frequencies that formed linear combinations of the semi-diurnal tides and their higher harmonics and the Coriolis frequency ($D_{2n} \pm f$). The spectrum for mooring BB 17 also showed a peak at diurnal frequencies, centred on the K_1 tidal frequency. The presence of spectral peaks at higher harmonics of the semidiurnal tides and at linear combinations of these frequencies with the Coriolis frequency is not unique for the slope region or thermocline in the Bay of Biscay. Van Haren et al. (2002) already reported the presence of such peaks in a spectrum derived from observations at a depth of 3819 m, 1000 m above the bottom in the Biscay Abyssal Plain. These are assumed to be caused by non-linear interaction, especially advective

of slower moving high-frequency waves by the dominant M_2 internal tides.

Because of the sampling period of 15 min for mooring BB 1 we were able to determine the spectra for that mooring up to frequencies well above the Brunt-Väisälä frequency in the main thermocline (29–44 cpd). The complete spectrum for this mooring (inset in Fig. 3(a)) shows an increase in the spectral slope at the lower boundary of this frequency range. For both moorings the background spectral continuum had an empirically determined $\omega^{-0.90(\pm 0.01)}$ character in the frequency range 2–24 cpd.

3.2. Spectra of vertical motion

The vertically averaged spectra of the vertical velocity W , measured with the ADCP, also show a near-white background spectral continuum, interspersed with spectral lines (Fig. 4). The spectral continuum is nearly constant until it shows a slight increase near the Brunt-Väisälä frequency. At higher frequencies (at least for BB 1 where these frequencies were resolved) a definite decrease of the

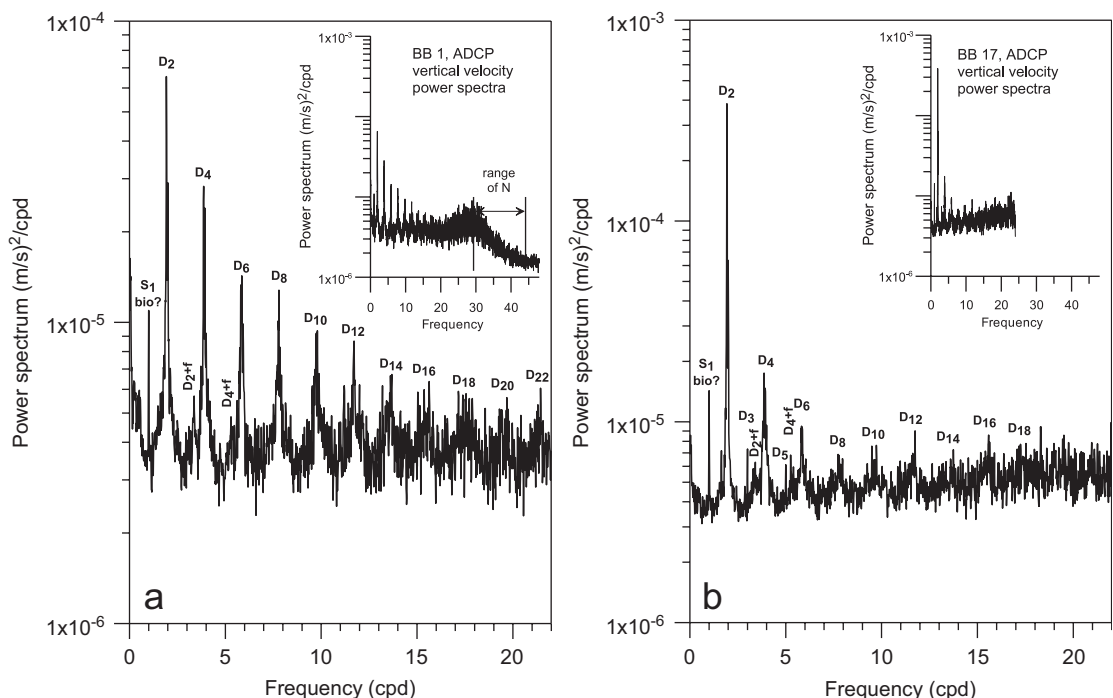


Fig. 4. Vertically averaged power spectra of the vertical velocity. The individual spectra per bin were averaged over bins 2–24 of mooring BB 1 (a) and bins 3–49 of mooring BB 17 (b). The insets show the complete spectra, the main figure the part of the spectra with pronounced peaks. In the inset of mooring BB 1 the range of the Brunt-Väisälä frequency N (mean plus or minus twice the standard deviation) in the depth range of the ADCP range is indicated with a two-headed arrow.

spectral values with increasing frequency occurred (see inset of Fig. 4(a)). At frequencies above 45 cpd, the spectral level approached the error level of the ADCP measurements. When we integrate the level of that high frequency spectral tail in Fig. 4(a) ($\sim 1.6 \cdot 10^{-6} \text{ m}^2 \text{ s}^{-2} \text{ cpd}^{-1}$) over the total frequency range (0–48 cpd), and then take the square root, we come to an estimate of the noise level in the vertical velocity of 0.9 cm s^{-1} . This value equals the standard deviation of the error velocity for mooring BB 1. The form of the spectral continuum agrees closely with the vertical displacement spectrum above the semi-diurnal frequencies, derived by Cairns (1975) from temperature observations with an oscillating mid-water float, multiplied by the square of the frequency. The multiplication is required to transform a displacement spectrum to a velocity spectrum. Recently, Lien et al. (2005) also published spectra of the vertical velocity in Luzon Strait that had a form similar to our Fig. 4. The level of the smooth background spectral continuum appeared to decrease upwards over the observational range by 45% and 30% for, respectively, BB 1 and 17.

Narrow spectral peaks were observed at the solar diurnal S_1 tidal frequency in the spectra of the vertical velocity. This is probably due to the diurnal vertical migration of biological scatterers (Weisberg and Parish, 1974). As diurnal migrations are quite discrete and offset from being perfectly sinusoidal the presence of higher harmonics of this S_1 signal is expected. These harmonics were indeed observed as narrow and small peaks at the S_2 to S_5 frequencies in the w-spectrum for BB 1, and up to S_4 for the w-spectrum for BB 17.

The dominant spectral peaks for the vertical motion were found at semi-diurnal tidal frequencies (D_2) and at higher harmonics of this frequency (D_{2n}). The vertical velocity measured at mooring BB 17 also showed relatively low but very narrow peaks at the D_3 and D_5 odd tidal harmonics, presumably indicating tidal advection of the diurnally moving scatterers. Linear combinations of the Coriolis frequency with tidal frequencies, e.g. D_2+f , and D_4+f , were also observed in the spectra of the vertical velocity while the inertial peak itself was absent. The absence of an f peak is to be expected, since near-inertial motion in the free water column is predominantly horizontal. The magnitude of the D_2 spectral peak at the semi-diurnal frequencies was an order of magnitude larger for mooring BB 17 compared with BB 1. In both cases this peak was

determined mainly by the semi-diurnal lunar M_2 tide.

Traditionally the vertical velocity, W , in an internal wave field was determined from temperature fluctuations, according to the relation (Krauss, 1966):

$$W = -\frac{\partial T}{\partial t} / \frac{\partial \bar{T}}{\partial z} \quad (1)$$

where $\partial T/\partial t$ is the time derivative of the observed temperature and $\partial \bar{T}/\partial z$ the mean vertical temperature gradient. We have compared the spectrum of the vertical velocity, determined from temperature measurements on the body of the ADCP from mooring BB 1, with the spectrum of the vertical velocity measured in the nearest ADCP bin 2, 40 m above the ADCP body (Fig. 5). Both spectra show similar spectral peaks of the same magnitude and the decrease of the background continuum spectrum in the Brunt-Väisälä frequency band. The

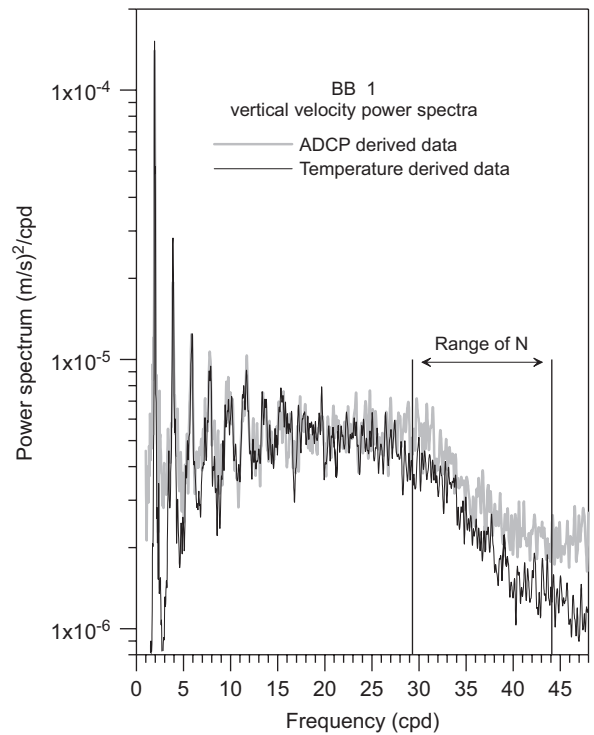


Fig. 5. Power spectra for the vertical velocity derived from the temperature sensor, mounted on the ADCP (thin black line), and from the velocity measured in bin 2.40 m above the temperature sensor (thick grey line). The ratio of the half-width spectral integral of the first 6 spectral peaks (T derived spectrum/ADCP derived spectrum) amounts to 1.02 (± 0.16). The range of the Brunt-Väisälä frequency, N , is indicated with a two-headed arrow.

main difference between the two spectra is the lower level of the background continuum of the temperature-derived spectrum at low frequencies (<4 cpd) and at the highest frequencies (>40 cpd). For a large part this difference can be explained by the influence of the noise in the ADCP signal. In order to determine whether the tidal peaks are well represented by the temperature fluctuations according to (1) we have determined the integral over the half-width of the first 6 spectral peaks. The mean ratio of the spectral integrals of the first 6 spectral peaks (temperature-derived spectrum/ADCP derived spectrum, semi-diurnal to bi-hourly peaks) amounted to 1.02 (± 0.16 standard deviation). This agreement of the variance of the tidal peaks in the ADCP-derived vertical velocity spectrum with those in the temperature-derived spectrum indicates that the determination of the vertical tidal velocity with the ADCP is reliable.

3.3. Coherent horizontal tides

In many models on internal tides and their generation the slight change in density stratification due to the seasonal cycle and meso-scale eddies has important consequences at larger distances from the generation area. Wave propagation along wave beams integrates the effects of stratification changes, so these may become dominant at larger distances from their source (Gerkema, 2001). Here we have assumed that our moorings over the continental slope are close to the generation area of internal tides. Then a considerable part of the observed internal wave motion is due to coherent baroclinic tidal waves (implying that amplitude and phase lag were persistent on the time scale of the mooring duration). To determine amplitude and phase of the internal tides we applied a harmonic analysis for the horizontal velocity measured in the ADCP bins. Each variable $x(t)$ was approximated by a function,

$$x(t) = \sum_{i=1,N} A_i \cos(\omega_i t - \phi_i) \quad (2)$$

with the constants A_i , ω_i and ϕ_i being, respectively the amplitude, angular frequency and phase lag of the i th of N tidal components (Emery and Thomson, 1997). In the analysis that we performed, the main semi-diurnal (M_2 , S_2 , and N_2) and diurnal (K_1 , O_1) as well as the M_4 and M_2S_2 harmonics from the D_4 band were used. Amplitude and phase lag were determined by means of a multiple

regression least-squares fit. The phase lag was defined with reference to $t = 0$ at 00:00 UTC on January 1 of the deployment year. For comparison with other high-frequency phenomena, separate high-pass-filtered current records were constructed that contained only variations at frequencies above 1/3 cpd. These high-pass currents represent about 80% of the total kinetic energy.

On average, the coherent harmonic tides contributed 54% of the observed high-frequency kinetic energy in both data sets. For both moorings, the M_2 tidal component gave the most important contribution, followed by the S_2 and the N_2 tidal components (order of magnitude of the amplitudes of 7, 3, and 1 cm s^{-1} , respectively). The tidal components from the D_1 and the D_4 bands had velocity amplitudes well below 1 cm s^{-1} .

At mooring BB 1 the variance of the horizontal velocity due to the M_2 component (Fig. 6(a)) was more or less constant from 720 m to about 900 m, halfway in the ADCP range ($42 \pm 1 \text{ cm}^2 \text{ s}^{-2}$). This value is at least twice the variance contribution expected from the barotropic M_2 tide. From 900 to 1075 m this variance increased to about $150 \text{ cm}^2 \text{ s}^{-2}$. The contribution of S_2 to the velocity variance was an order of magnitude smaller with a maximum at 850 m ($12 \text{ cm}^2 \text{ s}^{-2}$). The amplitudes of the N_2 tidal component were less than 2 cm s^{-1} at all depths, resulting in a variance of the order of $1\text{--}4 \text{ cm}^2 \text{ s}^{-2}$, definitely smaller than the M_2 and S_2 contributions. The M_2 tidal phase lag of both the east and north component (Fig. 6(b)) increased monotonically upwards, indicative of a downward component of the energy transport (Phillips, 1977). The M_2 phase-lag difference was 106° between 720 and 1075 m for the east component and 155° for the north component.

A numerical simulation of the superposition of a barotropic tide and a vertically propagating plane baroclinic tide shows that in order to get a monotonic vertical phase change larger than 90° , the baroclinic contribution has to be larger than the barotropic contribution. The observed relatively large phase change, $106\text{--}155^\circ$, shows that the dominant part of the observed tidal motion at BB 1 had a baroclinic character. One may assume that the low value of the current variance at ~ 900 m ($\sim 40 \text{ cm}^2 \text{ s}^{-2}$) occurs when the barotropic and baroclinic currents are in counter-phase, while the high value at 1075 m ($\sim 150 \text{ cm}^2 \text{ s}^{-2}$) occurs when the barotropic and baroclinic tides are in phase. Then the barotropic speed amplitude will amount to

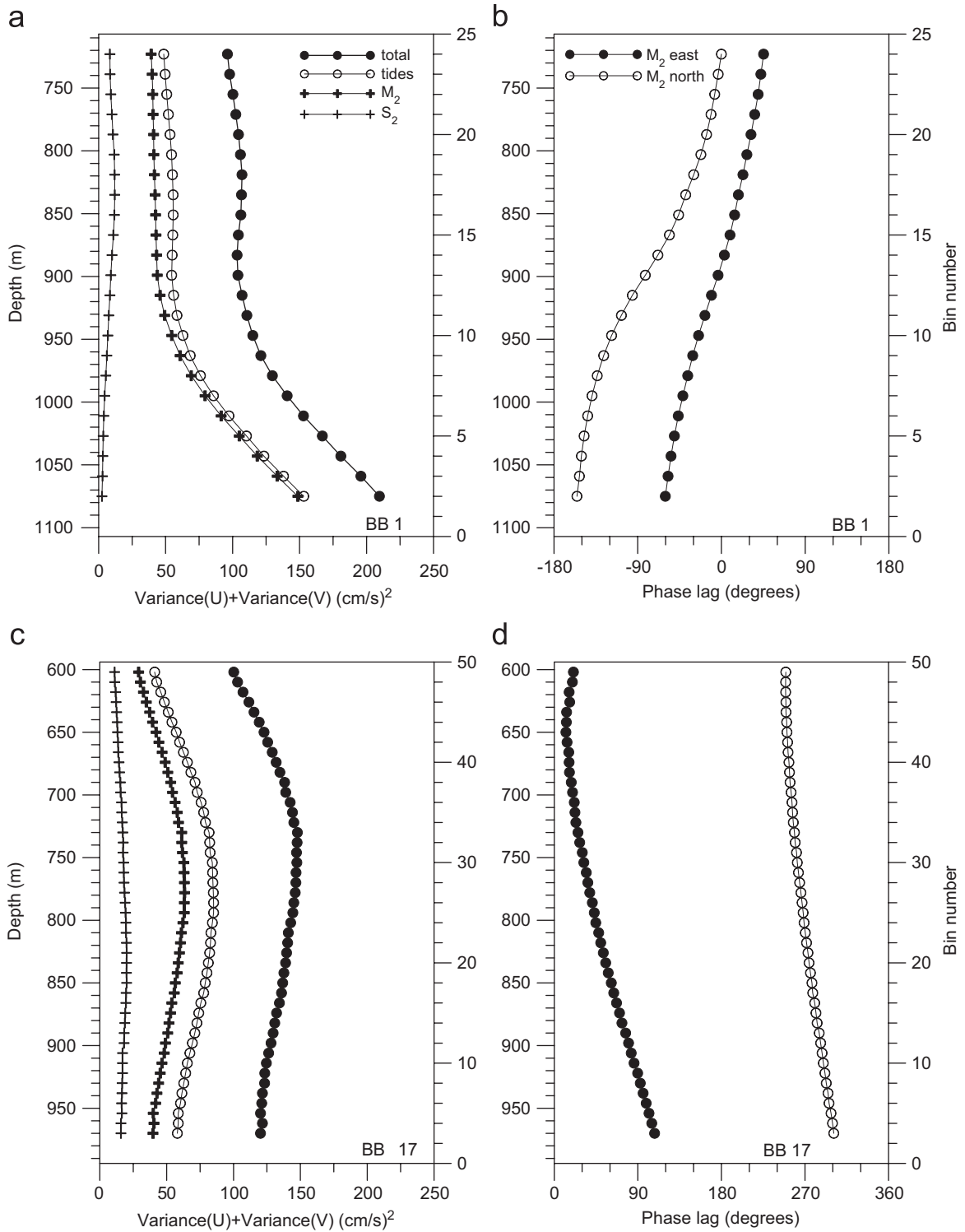


Fig. 6. Variance of the horizontal velocity (black circles), its total tidal contribution (open circles) and the contributions to the variance from the M_2 (thick crosses) and S_2 (thin crosses) harmonic tidal components (panel (a) for mooring BB 1 and panel (c) for mooring BB 17), and phase lag angles for the east (black symbols) and north (open symbols) components for the M_2 harmonic tidal component (panel (b) for mooring BB 1 and panel (c) for mooring BB 17).

$\sim 5.5 \text{ cm s}^{-1}$ and the baroclinic amplitude to $\sim 12 \text{ cm s}^{-1}$. This barotropic amplitude compares reasonably with the estimate of the upper bound of the barotropic tide at BB 1, introduced earlier. However, the phase information in Fig. 6(b) does not agree with this interpretation. With a larger amplitude for the baroclinic tide, the M_2 tide should be in counter-phase at both levels, not $57\text{--}73^\circ$ apart. Apparently a vertical change in the baroclinic current amplitude contributes to the observed variance structure. The observed gradient in the phase lag above 900 m, where the M_2 velocity variance was nearly constant, shows that also in that low-variance part of the water column the contribution of the baroclinic M_2 tide to the tidal variance is significant. The mean phase shift over the observational range suggests a vertical wavelength (distance over which the phase changes 360°) of 800–1200 m. Over 2/3 of the total kinetic energy in the M_2 band was located in the lowest 200 m of the observational range, an energy localization that, given the vertical phase change, cannot be attributed to interference of a barotropic and a vertically propagating plane baroclinic wave. According to model simulations by Gerkema et al. (2004) the internal M_2 tidal wave beam in the Bay of Biscay will be observed at a depth of ~ 1100 m at the BB 1 location, about 17 km from the 400 m isobath. These model simulations also show that most of the kinetic energy in internal wave beams is concentrated within a 180° phase lag interval. Thomas and Stevenson (1972) and Lighthill (1978) have derived a total phase change across a non-viscous 2-dimensional wave beam of only 180° , increasing up to about 360° for internal waves in a viscous fluid. Lam et al. (2004) and Gerkema et al. (2004) observed such baroclinic wave beams with a near -180° vertical phase shift across the beam in the upper 800 m of the ocean at nearby locations over the continental slope, similar to the model observations and the theoretical studies. Therefore, we interpret our observations as evidence for the presence of a deep tidal internal wave beam near 1075 m. The fact that 55% of the kinetic energy in this depth interval (71% at 1075 m) is phase-locked to the harmonic M_2 tide suggests that the source of the internal wave beam is quite nearby.

Mooring BB 17 showed a different vertical structure of the velocity variance and tidal phase lag. The total velocity variance had a maximum of $148 \text{ cm}^2 \text{ s}^{-2}$ at 725 m, while the contribution of the

harmonic M_2 tide had a variance maximum of $63 \text{ cm}^2 \text{ s}^{-2}$ only 50 m deeper (Fig. 6(c)). A current meter, mounted on the mooring at 1448 m, 50 m above the bottom, had an even higher M_2 variance of $83 \text{ cm}^2 \text{ s}^{-2}$. This maximum was over two times the minimum M_2 velocity variance observed near 600 m. The S_2 -related variance had a broad maximum of $20 \text{ cm}^2 \text{ s}^{-2}$ situated between 820 and 850 m. The contribution of the N_2 component was everywhere below $3 \text{ cm}^2 \text{ s}^{-2}$. The phase structure of the tides at mooring BB 17 also differed from that at BB 1. On the large scale the phase lag of both the M_2 and S_2 velocity components increased downwards, indicative for an upward energy transport (Fig. 6(d)). The M_2 phase shift between 970 and 650 m was found to be 96° and 52° for the east and north components, respectively. The M_2 phase lag, measured with the current meter at 1448 m (200° and 134° for the east and north components), suggests that between 968 (bin3) and 1448 m the phase lag gradient remained roughly similar to the gradient in the observational range, on average $23^\circ/100$ m. In the upper parts of the observational range the phase lag profile became more complicated, for the phase lag of the east component of the M_2 tide increased from 650 to 600 m, while in that depth range the phase lag of the M_2 north component was constant. This suggests a possible reversal of the vertical energy transport of the M_2 internal tide above 650 m. Vertical phase shifts of over 90° in the observational range and of over 180° between 650 and 1448 m suggest that also at this mooring a dominant part of the observed coherent M_2 tide was baroclinic. We have tried to reconstruct the observed vertical change of phase and tidal amplitude from a superposition of a vertically propagating plane internal wave and a barotropic tide. Satisfactory results were not possible unless we assumed a significant vertical change in the amplitude of the internal tide. Therefore, we will interpret the localization of the M_2 tidal energy near 775 m as a baroclinic wave beam, combined with a smaller barotropic tide.

The residual of the high-frequency variance ($> 1/3$ cpd), not explained by coherent tides, hardly varied vertically for either mooring, being $52 \pm 3 \text{ cm}^2 \text{ s}^{-2}$ and $62 \pm 3 \text{ cm}^2 \text{ s}^{-2}$ for moorings BB 1 and BB 17, respectively. This residual may be attributed to non-coherent tidal contributions induced by temporal changes in stratification and currents, as well as to near-inertial motions and internal waves at non-tidal frequencies.

3.4. Incoherent M_2 tide

The statistics, shown in Fig. 6, present the long-term mean vertical structure of the horizontal velocity field and of its tidal harmonics. On shorter time scales the velocity variance, the orientation of the tidal ellipse, and the vertical structure of the tidal phase and amplitude showed variability. Examples of the temporal and vertical variation of the velocity component in the direction of the major and the minor axis of the tidal ellipse during three successive days are shown in Fig. 7. The characteristic direction of the observed tidal ellipse for the 3-day period was defined as the direction in which the total variance of the velocity component for all ADCP bins was maximized. In these examples the semi-diurnal tide is dominant for the variability of the velocity structure. Between 24 and 27 November 1995 the vertical structure of the tide at BB 1 (Fig. 7a,b) resembled that of the mean semi-diurnal tide with most kinetic energy in the lower half of the observational range, although over these 3 days the core of high current variance descended 100 to 150 m in depth. The phase of the current increased upwards, similar to the phase lag of the M_2 harmonic tide, about 120° for the motion in the direction of the major axis of the tidal ellipse, and 180° in the direction of the minor axis. This phase shift agrees with a vertical wavelength of 800 to 1200 m. The major axis was oriented in the direction of 60° true north, about perpendicular to the continental slope, which runs from northwest to southeast.

From 18 to 21 January 1996 the major axis of the tidal ellipse was also directed more or less perpendicular to the local continental slope (65°). The velocity in that direction showed a monotonic and smooth vertical phase change, the motion at 1075 m depth leading the motion at 725 m by nearly 6 h (Fig. 7(c)). This phase change of nearly 180° can be interpreted as characteristic for vertically propagating internal waves with a wavelength of about 800 m. Contrary to the long-term mean M_2 motion, which showed a downward increase in amplitude, at least two high velocity cores were present. The most energetic of these cores was located near 800 m. The velocity component in the direction of the minor axis of the tidal ellipse showed two high-velocity cores (near ~ 780 and ~ 1050 m), moving more or less in counter-phase, with most of the phase change restricted to the 900 and 950 m interval (Fig. 7(d)).

At BB 17, from 13 to 16 January 1998, the velocity component in the direction of the major axis of the tidal ellipse (175°), also nearly perpendicular to the local continental slope, showed that during these 3 days most of the semi-diurnal tidal motion was concentrated between 625 and 800 m (Fig. 7(e)). The motion near 650 m was on average 1 h ahead of the motion at 900 m. The semi-diurnal motion perpendicular to the major axis of the tidal ellipse was also concentrated mainly in the upper half of the observational interval, with a secondary high velocity core near ~ 875 m (Fig. 7(f)). This velocity component had, similar to the cross-ellipse motion at BB 1 in January 1996, two high velocity cores nearly in counter-phase.

From 4 to 7 April 1998 the vertical velocity structure in the direction of the major axis of the tidal ellipse had more resemblance with the harmonic M_2 tide, with a high-velocity core halfway within the observational range (Fig. 7(g)). Similar to the harmonic M_2 tide, the motion at 625 m led the motion near 975 m by ~ 2.5 h. The structure of the motion in the direction of the minor axis (Fig. 7(h)) was more irregular, with one or two high-velocity cores at varying depths. In this direction the motion at the top of the observational range was also ahead of the motion at deeper levels.

The main variation in the velocity structure for short periods like those shown in Fig. 7 was in the magnitude and depth of the high velocity cores, with slight changes ($10\text{--}20^\circ$) in the orientation of the tidal ellipse. That variability showed a strong fortnightly spring-neap tide cycle, although significant variability was also observed at longer time scales. Averaged over a year that variation resulted in the smooth vertical change of amplitudes and phases of the harmonic tidal components shown in Fig. 6. The observed strong changes in amplitude of the semi-diurnal tides, and the limited vertical extent of the high-velocity cores, presented above, may be interpreted as internal wave beams that pass through the observational range.

The spring-neap tide cycle as well as changes in stratification and long term currents due to meso-scale eddies and seasonal and interannual variability may change the generation and propagation of internal tides, leading to local variations in amplitude and phase lag of the semi-diurnal internal tides, as is illustrated in Fig. 7. The latter parts of the internal tides are often referred to as incoherent internal tides (van Haren, 2004). To estimate the long-term variation of the incoherent M_2 tide and

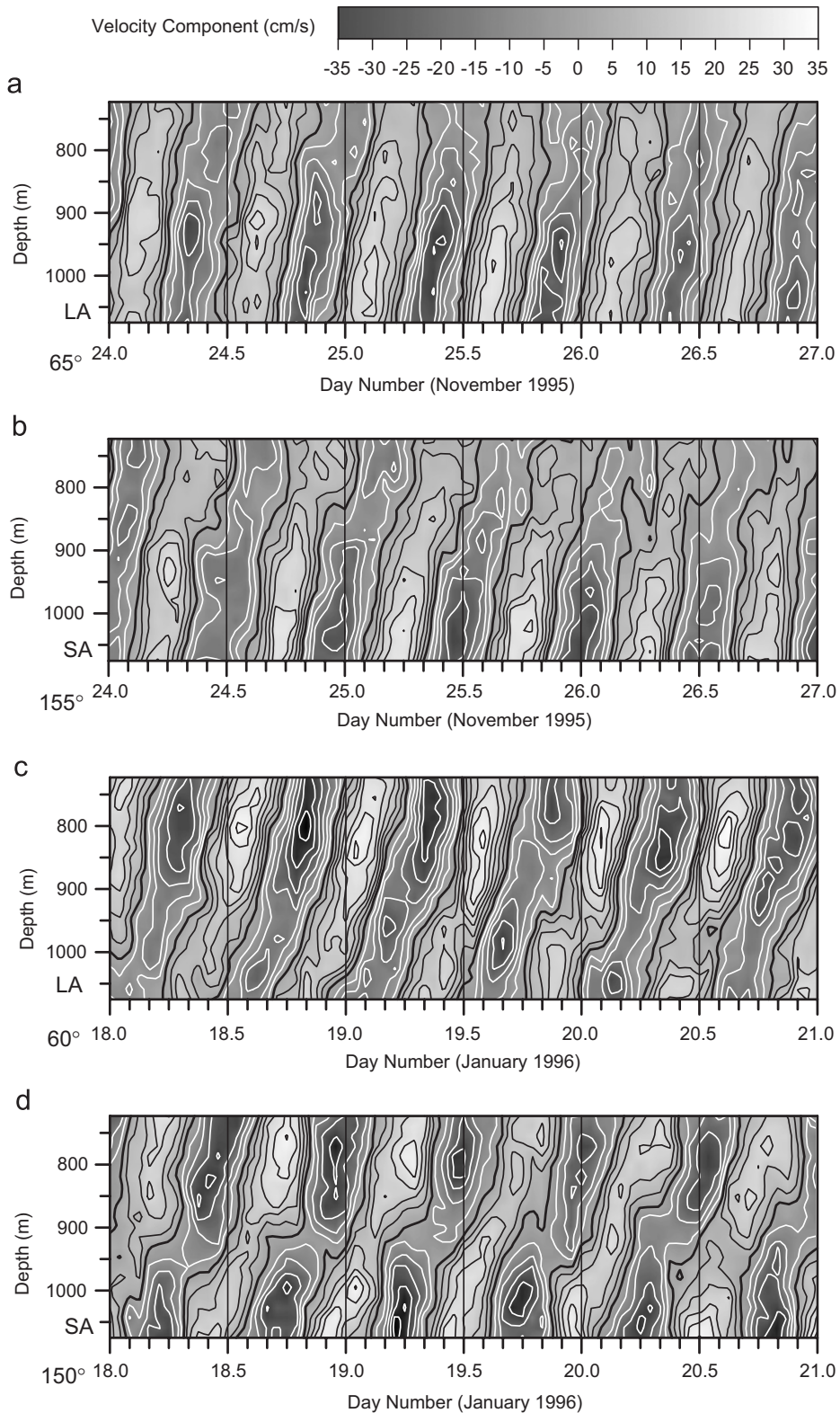


Fig. 7. Characteristic examples of the temporal-vertical distribution for 3 successive days of the horizontal velocity components in the directions of the long or major axis (LA) and the short or minor axis (SA) of the tidal ellipse. Panels (a and b) are from mooring BB 1 in November 1995, panels c and d from mooring BB 1 in January 1996, (e and f) from mooring BB 17 in January 1998, and (g and h) from mooring BB 17 in April 1998. The isolines are 5 cm s^{-1} apart, while the thick line is the isoline for zero velocity.

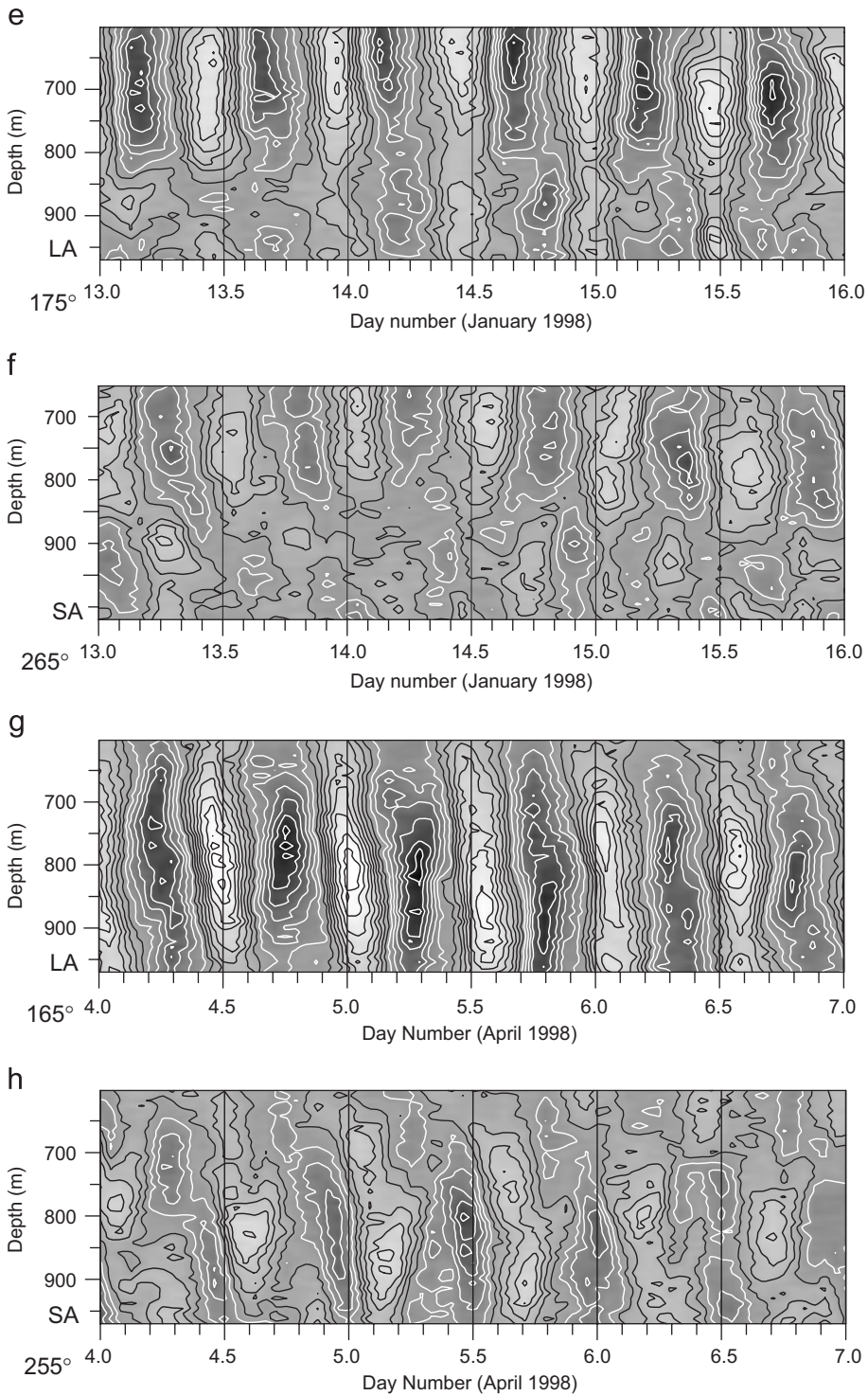


Fig. 7. (Continued)

its contribution to the total velocity variance we have determined the amplitude and phase of the M_2 tidal component for successive 14-day periods, with

a 7-day overlap (Figs. 8 and 9). The resulting amplitudes and phase lags contain contributions from the coherent as well as the incoherent tidal

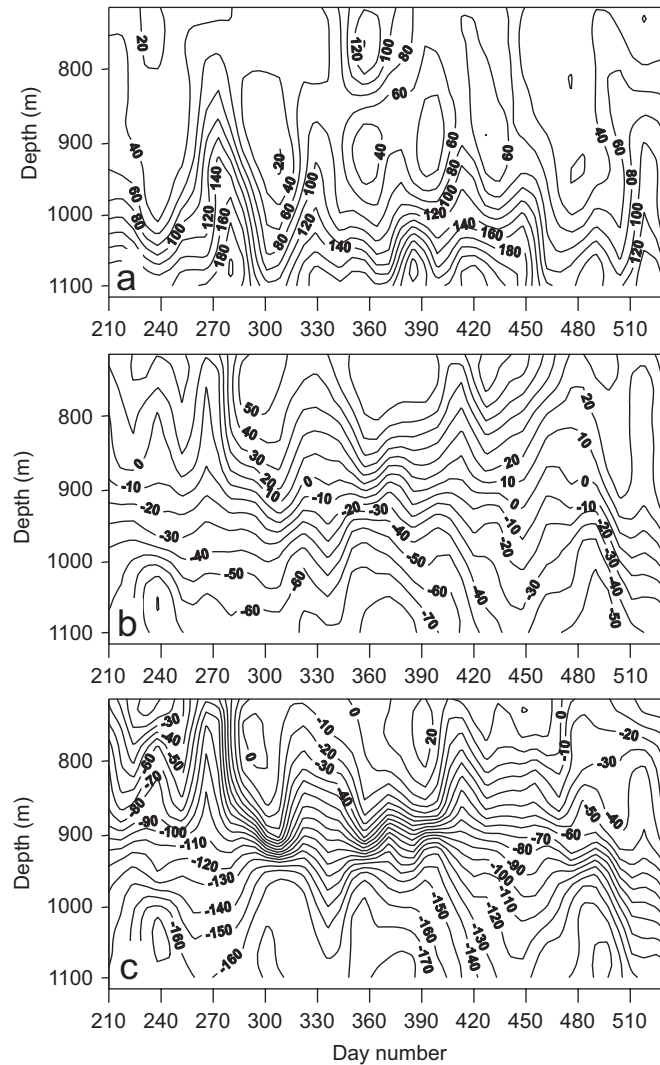


Fig. 8. Temporal change of the vertical structure of (a) the sum of the variances of the east and north velocity components (cm^2s^{-2}), (b) the phase lag (degrees) of the east and (c) the phase lag (degrees) of the north component of the M_2 tide, measured in mooring BB 1. January 1, 1995 equals day number 1. The data for these plots were obtained from a harmonic analysis over successive 14-day periods with a 7-day overlap.

waves. The velocity variance at mooring BB 1 shows that the kinetic energy of the M_2 internal waves changed by a factor of 2–5 with a characteristic time scale of 45 days (Fig. 8(a)). Occasionally, the sign of the vertical gradient of the velocity variance was inverted, e.g., during a high-energy phenomenon at the upper levels around day 360. The typical time scale of changes of the phase lag was also about 45 days (Fig. 8b,c). Inversions in the sign of the vertical gradient of the phase lag hardly occurred, and if so, they were smaller than 10° . This indicates that the direction of the vertical energy transport by the

internal tide stayed downwards throughout the mooring period.

The variability of variance and phase lag of the M_2 component at mooring BB 17 shows a similar variability with a characteristic 40-day time scale (Fig. 9). Occasionally patches of high variance with a vertical scale of about 200 m were observed in the observational range (Fig. 9(a)), often accompanied by abrupt changes in the phase lag (Fig. 9b,c). Similar to the mean phase lag change, the phase lags of both the east and north components showed a large-scale upward decrease, with only occasionally

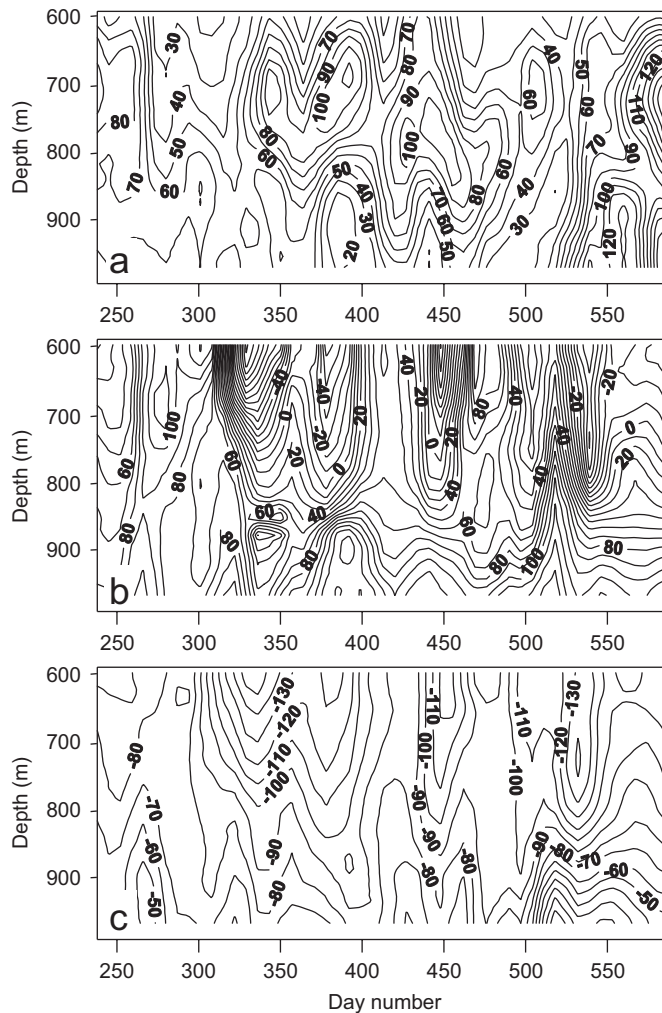


Fig. 9. Similar to Fig. 8, for mooring BB 17. January 1, 1997 equals day number 1.

a local inversion (e.g. around day 340 for the east component). This reflects the fact that most of the time the vertical component of the energy flux was directed upwards.

The characteristic 40–45-day time scale for the variability of the M_2 tide was probably associated with meso-scale eddy variability influencing the generation and propagation of internal tides in the Bay of Biscay (van Haren, 2004). The meso-scale temperature variability, measured with the ADCPs, can be considered to be characteristic for the baroclinic eddies. The characteristic time scale of this variability (from the mean peak-to-peak distance of the 7-day averaged signal) amounted to 47 days, of the same order as the 40- to 45-day time scale for the tidal variability. For both moorings the mean M_2 velocity variance derived from successive

14-day periods was about $13 \text{ cm}^2 \text{ s}^{-2}$ higher than for the long term coherent M_2 tide as shown in Fig. 6. The incoherent tides appear to contribute an extra 10% to the total high-frequency kinetic energy, enhancing the total tidal contribution to 64%.

3.5. Vertical component of the harmonic M_2 tide

The spectra of the vertical motion (Fig. 4) show that the semidiurnal M_2 tide is the dominant tidal contribution to the spectrum. A harmonic analysis of the vertical velocity was performed, which confirmed that the M_2 tide was by far the most important coherent tidal component, compared to other tidal frequencies. At mooring BB 1 the

coherent M_2 tide explained about 3.3% of the observed vertical motion (correlation = 0.18) for the lowest 160 m, where the strongest vertical motion was observed. At mooring BB 17, where the variance of W was distributed more evenly, about 13.5% of the variance of the vertical velocity was explained by the coherent M_2 tide (correlation = 0.37). Incorporation of the incoherent tidal signal from the harmonic analysis of successive 14-day periods, as described for the horizontal motion, increased these percentages to 4.4% at BB 1 and 15.8% at BB 17. These low tidal M_2 contributions to the vertical velocity, compared to the M_2 contribution to the horizontal velocity variance (~65%), were probably connected with the strong contributions to the variance of non-tidal internal waves, as reflected in the near-white character over a large part of the continuum spectrum of W (Fig. 4).

At mooring BB 1 the M_2 tide showed the largest contributions at the lowest depths, similar to the horizontal M_2 tide (Fig. 10(a)). The phase lag of the vertical M_2 tide increased upwards by 190° over 352 m (Fig. 10(b)). The phase difference between 1075 and 880 m, where the variance nearly reached its minimum, amounted to 91° . Thus the vertical distance of 195 m agreed here with about a quarter of the vertical wavelength (360° phase shift distance) of the internal tide, confirming the vertical wavelength estimate from the horizontal motion. In this depth interval the vertical motion was in phase with the velocity in the direction of approximately 30° true north, suggesting an opposite propagation direction of the M_2 internal wave beam towards 210° . That is more or less perpendicular to the nearby continental slope, which can be considered as the generation region for this internal wave beam. In the upper 100 m of the observational range the propagation direction of the internal tide was rotated towards the west. The maximum vertical tidal excursion near 1075 m, derived from the integration over half a tidal period of a 14-day harmonic M_2 vertical tidal velocity in the lowest ADCP bin, amounted to about 112 m, over three times the mean vertical excursion due to the harmonic M_2 tide, 34 m. Such variations were related to the variations in the internal M_2 tide, illustrated in Fig. 8.

The structure of the vertical tidal motion at mooring BB 17 differed strongly from that at mooring BB 1. The coherent vertical M_2 tide had a definitely larger variance than found for mooring

BB 1 with less vertical change than the variance of the horizontal tidal velocity (Fig. 10(c)). The ratio of the mean variance of the vertical velocity to the mean variance of the horizontal velocity was a factor of 10 larger for mooring BB 17 than for mooring BB 1. Although the overall vertical shift in phase lag for the coherent vertical M_2 tide had the same sign as for the horizontal tidal velocity, decreasing upwards, it was in magnitude much smaller, the maximum phase lag difference amounting to 27° (Fig. 10(d)). This implies that at mooring BB 17 the vertical tidal motion was nearly in phase over the whole observational range. Apparently the internal tides, which were responsible for the vertical tidal motion in the thermocline, had a relatively large vertical scale near mooring BB 17, at least of the order of the thickness of the thermocline. Heaving of the thermocline by the barotropic tide over the continental slope may be a likely interpretation of these results, although mooring BB 17 was relatively far (~20 km) from the 1000 m isobath. This heaving is part of the generation of internal tides (Lu et al., 2001). The vertical M_2 tidal velocity was in phase with the horizontal velocity component in the north-westward direction at the depth of the kinetic energy maximum, ~750 m. That direction is more or less in the direction of the local slope (Fig. 1). However, for heaving of the thermocline by the barotropic tide over a slope one can to first order expect the variance of the vertical velocity to increase with the square of the depth, and to be in phase over the whole water column. Most probably the deviation from a quadratic variance profile and the remaining vertical phase change are related to the co-existence of the baroclinic tide. The maximum vertical tidal excursion, derived from the 14-day harmonic M_2 vertical velocity varied from 129 m near 970 m, to 94 m above 750 m, nearly double the mean vertical excursion of 55 m, derived from the long-term coherent M_2 tide.

3.6. Near-inertial motion

Near-inertial waves in the ocean are assumed to be generated either locally as a response to local forcing, or remotely at lower latitudes as internal waves with a frequency close to the inertial frequency at the observation site (Fu, 1981). The local generation of inertial waves may be due to changes in the wind forcing at the sea surface (Ekman, 1905; Pollard and Millard, 1970) or due to

the geostrophic adjustment of currents in the ocean interior (Rossby, 1938; Gill, 1982; van Aken et al., 2005).

The near-inertial motion cannot be determined by a harmonic method like that used for tides because of its strongly variable phase and amplitude due to a

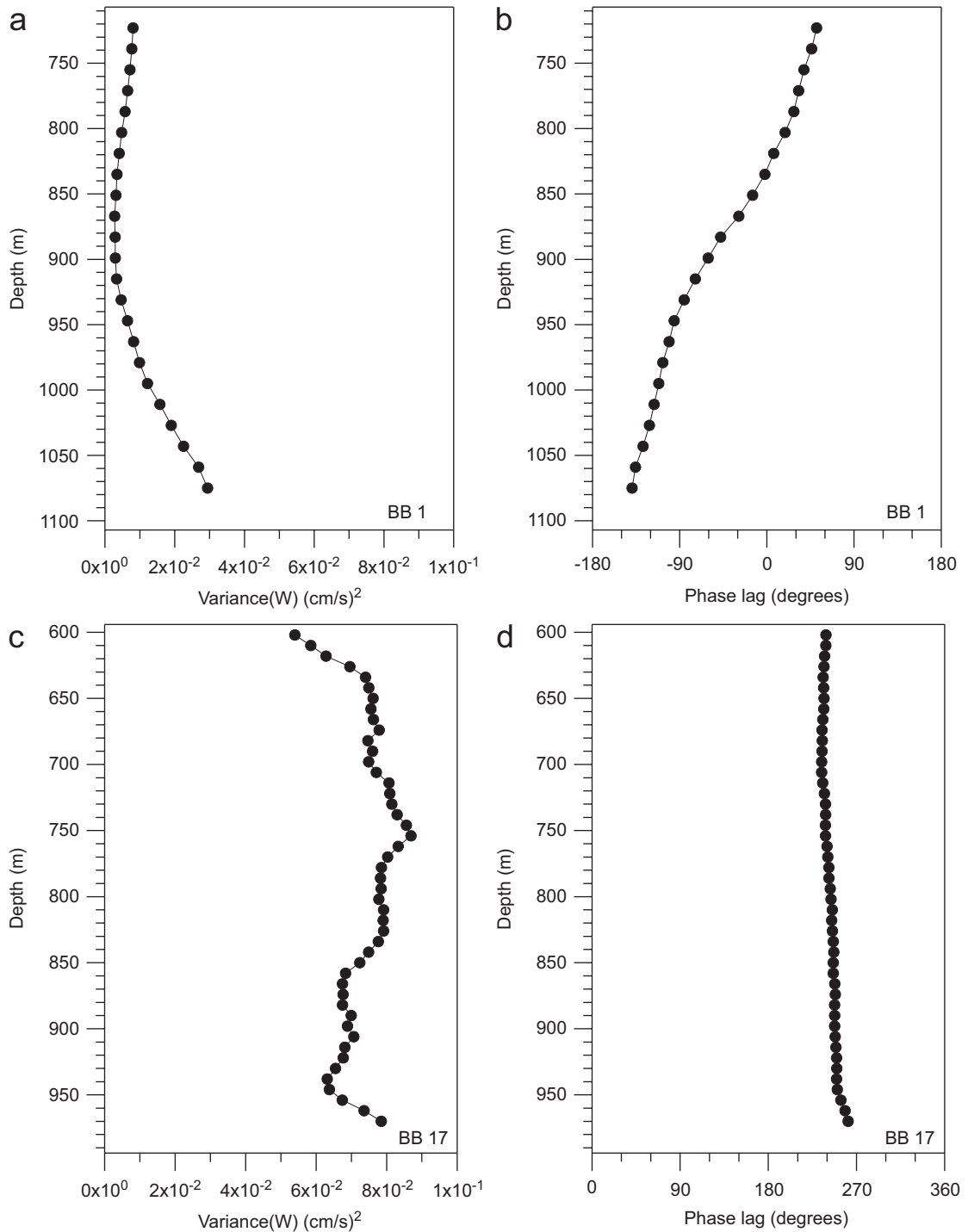


Fig. 10. Variance of the vertical velocity component measured with the ADCP in mooring BB 1 (a) and mooring BB 17 (c), as well as the phase lag angle for BB 1 (b) and BB 17 (d) as function of depth.

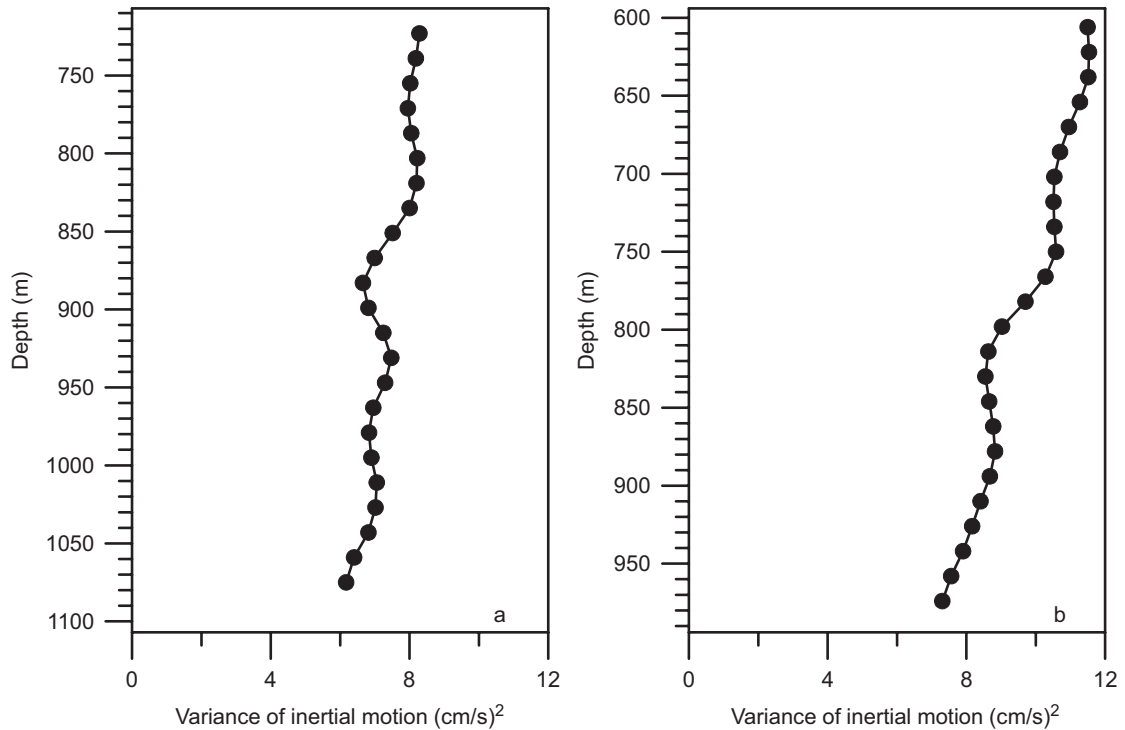


Fig. 11. Profiles of the summed variance of the east and north velocity component of the inertial band passed filtered signal for moorings BB 01 (a) and BB 17 (b). The filter was so designed that only the angular frequencies from $0.9 \times f$ to $1.1 \times f$ went through.

more or less random forcing. However, by an integration of the spectrum over a relatively narrow frequency band around the frequency f , we were able to determine the variance of the velocity related to the near-inertial motion. This variance appeared to depend on depth and slightly increased upwards (Fig. 11). The magnitude of the summed variance of the near-inertial motion (at frequencies $f \pm 10\%$) for mooring BB 1 and 17 amounted to, respectively, 7 and $10 \text{ cm}^2 \text{ s}^{-2}$. The mean contribution of the near-inertial waveband to the total high frequency ($> 1/3 \text{ cpd}$) kinetic energy was about 7%. The temporal variation of the variance in the near-inertial frequency band can also be determined from the band passed filtered data (Fig. 12). The variance time series shows that the variance at near-inertial frequencies was quite intermittent, with only 2 events above $50 \text{ cm}^2 \text{ s}^{-2}$ in a record of 11 months. Most inertial velocity variance, $8.3 \text{ cm}^2 \text{ s}^{-2}$, was found in the winter half year (ONDJFM) against only $3.1 \text{ cm}^2 \text{ s}^{-2}$ in the summer half year (AMJJAS), suggesting wind forcing as a generation process for near-inertial motion. However, in most cases (56%) strong energy near-inertial wave events had their

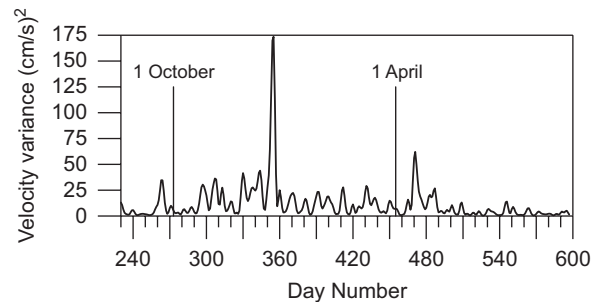


Fig. 12. The temporal development of the velocity variance in the $f \pm 10\%$ near-inertial wave band, average over the uppermost 55 m of the observational range in mooring BB 17. Day 1 is January 1 1997. The straight lines show the positions of the beginning and end of the winter half year.

strongest expression in the lower half of the observational range. This suggests that processes other than local wind forcing contribute to energy in the inertial wave band. Geostrophic adjustment of the deep boundary current near 1000 m depth over the continental slope was identified as a dominant source of energy for strong inertial events near Goban Spur in the northwestern Bay of Biscay (van Aken et al., 2005). Non-traditional Coriolis effects

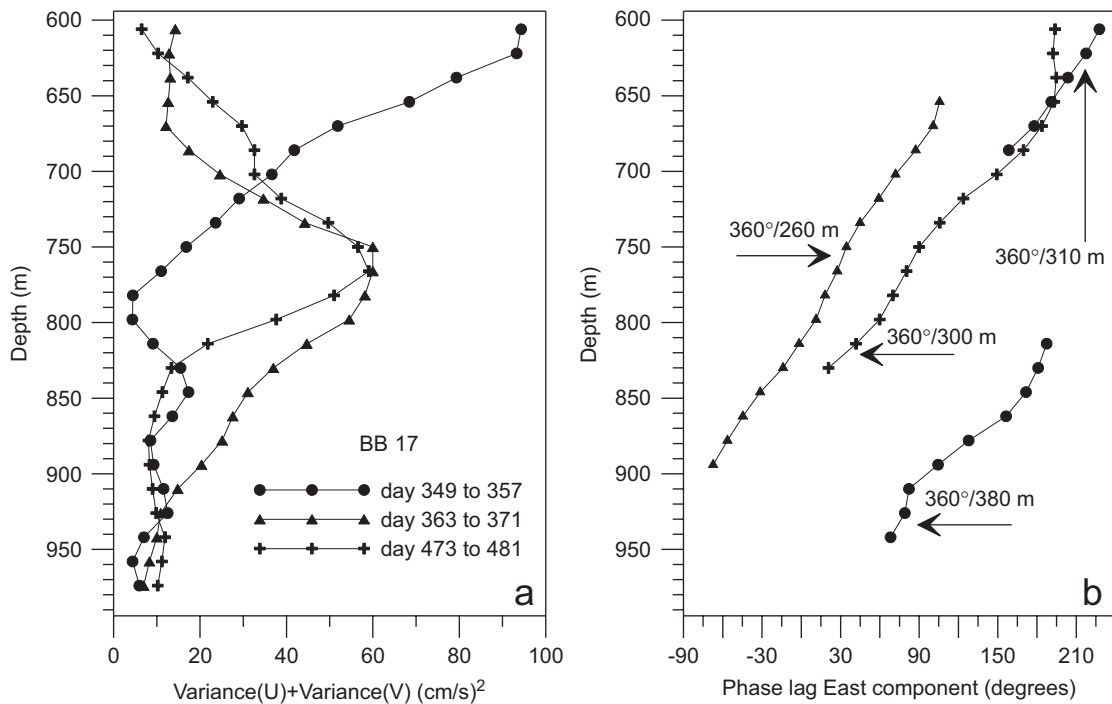


Fig. 13. Variance profiles of the velocity components of the approximated inertial waves during three high inertial energy events at mooring BB 17 where the strongest near-inertial events were observed (a), and the corresponding phase lag profile of the east component of the waves (b).

are also considered to be responsible for the enhancement and near-bottom trapping of near inertial waves (Maas, 2001; Gerkema and Shrira, 2005). As can be expected for near-inertial motions, the horizontal velocity vector followed a near-circular path and rotated clockwise in time.

The strongest near-inertial frequency events were found in the data from mooring BB 17. For three high-energy inertial events, observed at mooring BB 17, we have tried to resolve the vertical amplitude and phase structure by approximating over 7-day periods the inertial band-passed ($f \pm 10\%$) velocity signal $u(t)$, $v(t)$ by a least squares fit with a sinusoidal curve defined as

$$[u, v] = [U, V] \cos(ft - \phi_{u,v}), \quad (3)$$

where $U(z)$ and $V(z)$ are the vertically varying amplitudes of the inertial waves and $\phi_u(z)$, $\phi_v(z)$ the corresponding phase lags. The events chosen were: 15–22 December 1997 (day 349–356), 29 December 1997–5 January 1998 (day 363–370) and 18–25 April 1998 (day 473–480). The velocity variance related to the inertial oscillation, $(U^2 + V^2)/2$ (Fig. 13(a)), showed for day 349–356 a maximum just below the top of the observational range near 600 m and a

slightly enhanced variance region between 800 and 950 m. For the other two periods the variance maxima were well embedded within the observational range. The typical mean half width of these variance peaks was estimated to be 120 m. In these variance peaks the mean phase lag difference between east and north components of the velocity is $90.7^\circ (\pm 1.1^\circ \text{ standard error})$, consistent with a circular clockwise rotation of the velocity vector. In all four variance peaks the phase lag of the near-inertial oscillations increased upwards, indicative of a downward energy transport. The rate of phase increase varied from $360^\circ/380 \text{ m}$ to $360^\circ/260 \text{ m}$. A mean vertical wavelength (360° phase shift distance), estimated from these wave numbers, amounted to 380 m. The approximate mean thickness of the variance peaks, 240 m (twice the half width), appeared to be definitely less than this wavelength.

3.7. Vertical current shear

Internal and near-inertial waves are important phenomena for the transport of mechanical energy through the ocean. That energy ultimately can be

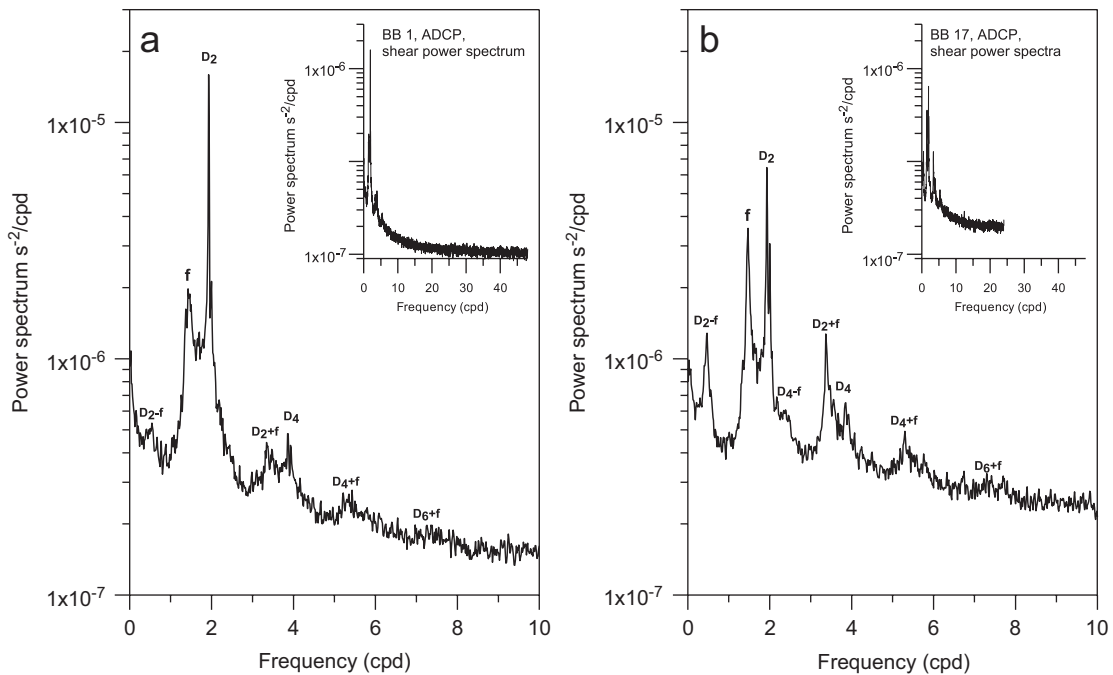


Fig. 14. Summed power spectra of the east and north components of the velocity shear over a 16 m vertical interval, averaged over all available bin pairs, for moorings BB 1 (a) and BB 17 (b). The insets show the complete spectra, the main figure the parts of the spectra with pronounced peaks. The identified spectral peaks at tidal and inertial frequencies, their higher harmonics and linear combinations are indicated.

made available for mixing in the interior of the stratified ocean by the shear production of turbulent kinetic energy. For the analysis of the phenomena responsible for the generation of turbulence, we have derived the vertical current shear from neighbouring 16-m ADCP bins and calculated the individual shear spectra, summed these over the east and north components, and averaged them for all the available depth intervals (Fig. 14). For mooring BB 17 velocity values every 16 m were obtained by averaging over two neighbouring 8-m ADCP bins. Determining the shear over a vertical distance of 16 m relates the shear values to phenomena with a vertical wavelength larger than twice this distance. The shear, related to smaller scale phenomena is partly missed by this method, and partly aliased to larger scales. For both moorings the variance of the velocity difference per component over 16 m was well above the noise level, derived from the error velocity, up to a factor of 60 for mooring BB 17.

The shear spectra show a number of peaks that can be identified with specific combinations of tidal and inertial frequencies (Fig. 14). At frequencies above 20 cpd the spectra level off to nearly constant values. For mooring BB 17 this level is about twice

the high-frequency spectrum for mooring BB 1. For both moorings the level of the background spectral continuum appeared to decrease monotonically upwards over the observational range of nearly 400 m, with a factor 1.4 and 1.9 for BB 1 and 17, respectively.

The main spectral peaks for both moorings were found at the frequencies of the semi-diurnal tides D_2 (both M_2 and S_2 peaks) and at the inertial frequency f . The shear variance in the inertial-semidiurnal frequency band (1 to 2.5 cpd) at mooring BB 1 had a slight maximum near 900 m, about 50% higher than near 700 and 1100 m. At mooring BB 17 the shear variance in that frequency band decreased monotonically upwards with about 25% over the observational range. Spectral peaks were also found at the first higher harmonic of the semi-diurnal frequencies D_4 . All other peaks involve sums and differences of tidal frequencies with f , i.e. D_2-f outside the internal wave band and D_4-f , D_2+f , D_4+f and D_6+f in the internal wave band. The peaks at frequencies involving f are larger in the shear spectrum than in the velocity spectrum. This is especially clear in the spectrum for BB 17 (Fig. 14(b)), where the f , D_2-f and D_2+f peaks

form three of the five highest spectral peaks. The equal magnitudes of the D_2-f and D_2+f shear peaks suggest support for the hypothesis of so-called “fine-structure contamination” as cause for these peaks (Alford, 2001). Such contamination is caused by vertical advection by the main internal tide of the near-inertial current shear, which has a small vertical length scale. The prominence of the f -related shear suggests that the velocity structure at the inertial frequency has a relatively small vertical scale compared with the tidal frequencies. One can define such a characteristic vertical length L as

$$L_z = 2\pi \left(\int_B P_v df / \int_B P_{sh} df \right)^{1/2}, \quad (4)$$

where the power spectra of velocity, P_v and of shear, P_{sh} , are integrated over an appropriate frequency band B . For plane waves this definition agrees with the vertical wavelength.

The estimates of L_z for the different frequency bands (Table 2) show that the characteristic length scale is largest for the semi-diurnal tides, $O(L) = 900$ m, followed by the quarter-diurnal harmonics, $O(L) = 430$ m. The near-inertial waves have a smaller vertical length scale than the internal tides, $O(L_f) = 310$ m, while for the frequency bands formed by combinations of the inertial and tidal frequencies the smallest vertical length scales are found, $O(L) = 180$ m. This result indicates that while the internal tides are very dominant for the variance of the horizontal velocity, the near-inertial wave band may be more important for the generation of shear-induced turbulence.

A criterion for the onset of turbulence that derives its energy from the velocity shear is based

on the gradient Richardson number Ri_g , defined as:

$$Ri_g = \frac{N^2}{\sqrt{(\partial u / \partial z)^2 + (\partial v / \partial z)^2}}. \quad (5)$$

If Ri_g descends below a critical value (somewhere between 0.25 and 1.0; Turner, 1973) turbulent mixing will maintain a vertical mass transport. In waves with circularly rotating shear vectors, like the near-inertial waves, the high shear regime is continuously present as has been observed in the stratified North Sea (van Haren, 2000). We have determined the Richardson numbers from the shear measured with the ADCP over a vertical distance $\Delta z = 16$ m, averaged over 15 min for mooring BB 1 and over 30 min for mooring BB 17. For mooring BB 1 Ri_g is less than 1 for 41% of the time, and less than 0.5 for 17% of the time, while for mooring BB 17 these percentages amounts to 39% and 15%, respectively. For both moorings the percentage of time that $Ri_g < 1$ decreased smoothly upwards over the observational range by about 10%. Although the long-term average percentage of the time that low Richardson numbers occur varies smoothly with depth, its distribution in space and time was strongly intermittent at shorter time scales, similar to the occurrence of strong near-inertial events. And it is these events that generate high shear and low Richardson numbers because of their relatively small vertical length scale. This frequency range between f and D_4+f provides 57% of the shear variance for mooring BB 1 and 49% for mooring BB 17. Apparently the shear related to the near-inertial waves, and their combinations with tidal frequencies, are a main factor for the large fraction of the time when the low Richardson number allows turbulent mixing.

The near-inertial velocity variance shown in Fig. 12 was positively correlated with the time fraction that Ri_g was below 0.5 in the same depth interval ($R = 0.58$). Many strong near-inertial events could be linked to low Ri_g events. As an example Fig. 15(a) shows the temporally coincident occurrence of a strong near-inertial event in the upper 55 m of the observational range in December 1997. The vertical structure of strong near-inertial events and of low Ri_g events were repeatedly also quite similar. This is illustrated for the event in April 1998 (Fig. 15(b)). This result confirms the relative importance of the near-inertial wave band for turbulent mixing in the ocean.

Table 2
Vertical wavelength L_z (360° vertical phase shift), according to (4), determined for different frequency bands

Mooring	BB 1	BB 17
Frequency Band	L_z (m)	L_z (m)
D_2-f	194	194
f	276	339
D_2	791	1011
D_4-f	200	
D_2+f	200	220
D_4	433	427
D_4+f	170	163
D_6+f	144	132

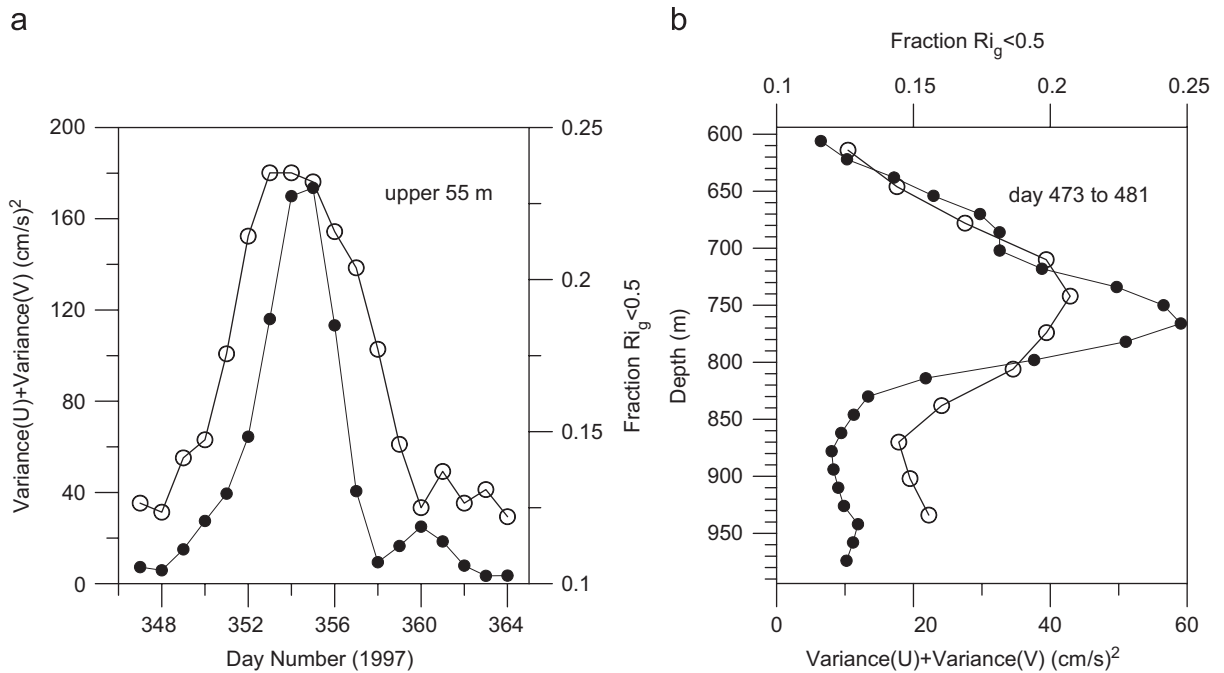


Fig. 15. Examples of the coincidence in time (a) and space (b) of strong near-inertial events (black dots) and events with a large time fraction with low Richardson numbers ($Ri_g < 0.5$, open symbols). The near-inertial event in (a) is the strongest event shown in Fig. 12. The event in (b) is also shown in Fig. 13. The fraction of time with low Richardson number is a 7-day running mean value.

4. Discussion

Spectral analysis of the ADCP data showed that tidal motion was a dominant feature in the permanent thermocline over the continental slope of the Bay of Biscay. The harmonic analysis of the ADCP data revealed that over 50% of the high-frequency ($> 1/3$ cpd) kinetic energy can be attributed to coherent semi-diurnal tides with yearlong constant phase lag and amplitude. Short-term velocity records, however, showed a considerable variation of the semi-diurnal motion, which was attributed to incoherent tides with time-varying amplitude and phase lag. When incoherent tidal contributions were incorporated, about 2/3 of the high-frequency kinetic energy could be explained. The horizontal harmonic semi-diurnal tidal motion in the thermocline appeared to have a definitive vertical structure in amplitude and phase. For mooring BB 1 the highest M_2 amplitude was found near 1075 m depth, for mooring BB 17 near 750 m. The phase lag of the tidal signal varied significantly in the vertical, up to $106^\circ/350$ m and $155^\circ/350$ m for, respectively, the M_2 east and north velocity components of mooring BB 1. The observed vertical change of phase lag and velocity variance indicated

that the largest part of the tidal motion had the character of propagating internal waves. The restricted vertical range of the variance maxima of the horizontal velocity suggested that the internal tidal motion was largely organized in wave beams of limited vertical extent, about 400 m, probably emerging from a nearby generation area on the continental slope. This interpretation agrees with earlier observations and modelling results for nearby positions in the Bay of Biscay (Pingree and New, 1991; Lam et al., 2004; Gerkema et al., 2004).

Because of the predominantly white noise character of the spectral continuum of the vertical velocity spectrum, the tidal peaks in this spectrum were less dominant than the tidal peaks in the spectrum of the horizontal velocity. Nevertheless, the semi-diurnal and higher harmonics were clearly recognizable in the vertical velocity spectra. Harmonic analysis of the M_2 contribution to the vertical motion showed a vertical distribution of the velocity variance and phase lag in general agreement with the distribution of the velocity variance for the horizontal motion. Including incoherent tides, the M_2 band contributed on the order of 5 to 15% to the total variance of the vertical velocity. This agreed with a maximum vertical tidal excursion in

the thermocline of about 110 to 130 m. Unpublished deep (1200 m) CTD yoyo time series from the Bay of Biscay over a tidal period confirm the existence of such large internal tidal waves. Most of the remaining vertical velocity variance was connected with the spectral continuum. Probably only a limited part of this continuum was related to instrumental noise, given the agreement of the temperature derived spectrum with the ADCP derived spectrum (Fig. 5) and the agreement of the spectral continuum with the spectral form observed by Cairns (1975) and Lien et al. (2005).

Assuming that the M_2 velocity signal at mooring BB 1 was purely baroclinic, the observed vertical change of the phase shift was equivalent to a vertical wavelength of about 800 m, about twice the estimated vertical scale of the tidal wave beam. This agreed in magnitude with the vertical wavelength derived from the harmonic vertical motion. The vertical gradient of the observed phase lag indicated that at mooring BB 1 the M_2 tidal energy was transported downwards. From the correlation between horizontal and vertical motion it was derived that the horizontal propagation direction of the internal tidal wave beam was 210° true north, away from a probable generation region over the nearby upper continental slope.

For mooring BB 17 an upward energy transport was derived from the vertical change of the phase lag of the horizontal M_2 tidal motion. However, the strong semi-diurnal vertical motion at different depths was nearly in phase. This was probably caused by heaving of the thermocline water due to tidal motion northwestward over the complicated sloping topography near the Meriadzek Plateau. Apparently Mooring BB 17 was located in a region where internal tides were generated or reflected.

The presence of near-inertial waves could be recognized from a spectral peak at the Coriolis frequency. A seasonal cycle of near-inertial kinetic energy could be recognized, with most energy in the winter period. This may be due to stronger wind forcing of inertial motion in winter. However, the vertical distribution of strong near-inertial events suggested that a considerable part of the near-inertial energy entered the observational range laterally or from below, possibly forced by geostrophic adjustment events. The analysis of individual near-inertial wave events showed a characteristic vertical structure with relatively strong current shear. During these events the waves also seemed to be organized in wave packets with a

vertical extent of about 240 m. The rate of change of the phase suggested a mean vertical wavelength of about 380 m. So the width of the near-inertial wave beam appears to be smaller than the vertical wavelength, a result that compares well with our findings for the semi-diurnal internal tides.

The vertical velocity shear in the near-inertial frequency band was more important than that in the tidal bands because of the small vertical extent of the inertial wave packets. Many strong near-inertial wave events appeared to be coincident in space and time with low Ri_g events. The resulting annual mean gradient Richardson number in the main thermocline turned out to be close to the critical value. This suggests that over the continental slope of the Bay of Biscay the circumstances are favourable for a nearly permanent maintenance of turbulent mixing, driven by the energy supplied by the inertia-gravity wave band, especially at near-inertial frequencies. In order to improve the local parameterization of mixing in ocean general circulation models, we should improve the understanding of the roles and distribution of both internal tides and near-inertial waves and their generation, transmission and breaking.

Acknowledgements

This research was funded by the board for Earth and Life Sciences (ALW) of the foundation for Netherlands Scientific Research (NWO) as part of the Bay of Biscay Boundary project. The three anonymous reviewers, who made comments on the initial manuscript, are acknowledged for their efforts, which led to numerous improvements.

References

- Alford, M.H., 2001. Fine-structure contamination: observations and a model of a simple two-wave case. *Journal of Physical Oceanography* 31, 2645–2649.
- Baines, P.G., 1982. On internal tide generation models. *Deep-Sea Research* 29, 307–338.
- Bendat, J.S., Piersol, A.G., 1986. *Random Data*, second ed. Wiley-Interscience, New York, pp. 566.
- Cairns, J.L., 1975. Internal wave measurements from a midwater float. *Journal of Geophysical Research* 80, 299–306.
- Ekman, V.W., 1905. On the influence of the earth's rotation on ocean currents. *Arkiv Mat. Astron. Fys.* 2, 1–52.
- Emery, W.J., Thomson, R.E., 1997. *Data analysis methods in physical oceanography*. Pergamon, Kent, pp. 634.
- Fjeldstad, J.E., 1963. internal waves of tidal origin. *Goefysiske Publikasjoner. Geophysica Norvegica* 25 (5), 1–73.

- Frankignoul, C., 1974. A cautionary note on the spectral analysis of short internal wave records. *Journal of Geophysical Research* 79, 3459–3462.
- Fu, L.-L., 1981. Observations and models of inertial waves in the deep ocean. *Reviews of Geophysics and Space Physics* 19, 141–170.
- Garrett, C., Munk, W., 1975. Space-time scales of internal waves: a progress report. *Journal of Geophysical Research* 80, 291–297.
- Garrett, C., Munk, W., 1972. Space-time scales of internal waves. *Geophysical Fluid Dynamics* 2, 225–264.
- Gerkema, T., 2001. Internal and interfacial tides: beam scattering and local generation of solitary waves. *Journal of Marine Research* 59, 227–255.
- Gerkema, T., Lam, F.-P.A., Maas, L.R.M., 2004. Internal tides in the Bay of Biscay: conversion rates and seasonal effects. *Deep-Sea Research II* 51, 2995–3008.
- Gerkema, T., Shrira, V.I., 2005. Near-inertial waves in the ocean: beyond the traditional approximation. *Journal of Fluid Mechanics* 529, 195–219.
- Gill, A.E., 1982. *Atmosphere-Ocean Dynamics*. International Geophysics Series, 30. Academic Press, New York, 662pp.
- Hayes, S., Halpern, D., 1976. Observations of internal waves and coastal upwelling off the Oregon coast. *Journal of Marine Research* 34, 247–267.
- Krauss, W., 1966. *Interne Wellen*. Gebrüder Borntraeger, Berlin, pp. 248.
- Lam, F.-P.A., Maas, L.R.M., Gerkema, T., 2004. Spatial structure of tidal and residual currents as observed over the shelf break in the Bay of Biscay. *Deep-Sea Research I* 51, 1075–1096.
- LeBlond, P.H., and Mysak, L.A., 1978. *Waves in the ocean*. Elsevier Oceanography Series, 20, Elsevier Scientific Publishing Company, Amsterdam, 602pp.
- Ledwell, J.L., Montgomery, E.T., Polzin, K.L., St. Laurent, L.C., Schmitt, R.W., Toole, J.M., 2000. Evidence for enhanced mixing over rough topography in the abyssal ocean. *Nature* 403 (6766), 179–182.
- Lien, R.-C., Tang, T.Y., Chang, M.H., D'Asaro, E.A., 2005. Energy of nonlinear internal waves in the South China Sea. *Geophysical Research Letters* 32, L05615.
- Lighthill, M.J., 1978. *Waves in Fluids*. Cambridge University Press, Cambridge, 504pp.
- Lu, Y., Wright, D.G., Brickman, D., 2001. Internal tide generation over topography: experiments with a free-surface z -level ocean model. *Journal of Atmospheric and Oceanic Technology* 18, 1076–1091.
- Maas, L.R.M., 2001. Wave focusing and ensuing mean flow due to symmetry breaking in rotating fluids. *Journal of Fluid Mechanics* 437, 13–28.
- Munk, W., Wunsch, C., 1998. Abyssal recipes II: energetics of tidal and wind mixing. *Deep-Sea Research I* 45, 1976–2009.
- Pérenne, N., Pichon, A., 1999. Effect of barotropic tidal rectification on low-frequency circulation near the shelf break in the northern Bay of Biscay. *Journal of Geophysical Research* 104, 13489–13506.
- Phillips, O.M., 1977. *The dynamics of the upper ocean*. (second edition) Cambridge Monographs on Mechanics and Applied Mathematics, Cambridge University Press, Cambridge, 336pp.
- Pingree, R.D., Griffiths, D.K., Mardell, G.T., 1983. The structure of the internal tide at the Celtic Sea shelf break. *Journal of the Marine Biological Association of the United Kingdom* 64, 99–113.
- Pingree, R.D., New, A.L., 1991. Abyssal penetration and bottom reflection of internal tidal energy in the Bay of Biscay. *Journal of Physical Oceanography* 21, 28–39.
- Pingree, R.D., New, A.L., 1995. Structure, seasonal development and sunglint spatial coherence of the internal tide on the Celtic and Armorican shelves and the Bay of Biscay. *Deep-Sea Research I* 42, 245–284.
- Pollard, R.T., Millard, R.C., 1970. Comparison between observed and simulated wind-generated inertial oscillations. *Deep-Sea Research* 17, 813–821.
- Polzin, K.L., Toole, J.M., Ledwell, J.R., Schmitt, R.W., 1997. *Science*, 276, 93–96.
- Rossby, C.G., 1938. On the mutual adjustment of pressure and velocity distributions in certain simple current systems, II. *Journal of Marine Research* 1, 239–263.
- Shcherbina, A.Y., Talley, L.D., Firing, E., Hacker, P., 2003. Near-surface frontal zone trapping and deep upward propagation of internal wave energy in the Japan/East Sea. *Journal of Physical Oceanography* 33, 900–912.
- Thomas, N.H., Stevenson, T.N., 1972. A similarity solution for viscous internal waves. *Journal of Fluid Mechanics* 61, 495–506.
- Turner, J.S., 1973. *Buoyancy Effects in Fluids*. Cambridge University Press, Cambridge, UK, pp. 367.
- van Aken, H.M., Maas, L.R.M., van Haren, H., 2005. Observations of Inertial Wave Events near the Continental Slope off Goban Spur. *Journal of Physical Oceanography* 35, 1329–1340.
- van Haren, H., 2000. Properties of vertical current shear across stratification in the North Sea. *Journal of Marine Research* 58, 465–491.
- van Haren, H., 2004. Incoherent internal tidal currents in the deep-ocean. *Ocean Dynamics* 54, 66–76.
- van Haren, H., Maas, L.R.M., van Aken, H.M., 2002. On the nature of internal wave spectra near a continental slope. *Geophysical Research Letters* 29.
- Weisberg, J., Parish, H., 1974. *Introductory Oceanography*. McGraw-Hill Book Company, New York, pp. 320.